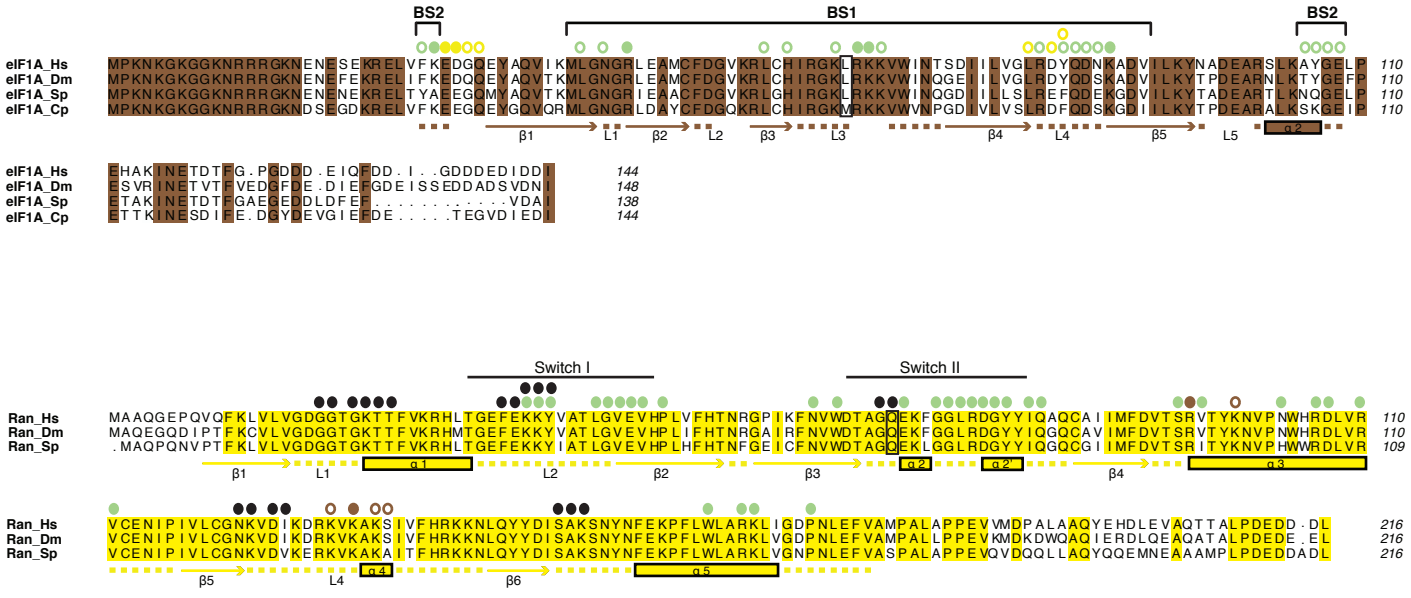

Supplementary Figure 1A. Structure-based sequence aligment of eIF1A and RanGTP.
The alignment shows eIF1A and RanGTP orthologues from *H. sapiens* (Hs), *D. melanogaster* (Dm) and *S. pombe* (Sp). The eIF1A alignment is complemented with the orthologue from *C. parvum* (Cp), which was used as a structural model in MODELLER. The conserved residues are highlighted in brown and yellow, respectively. The secondary structure elements are indicated as rectangles for α-helices and arrows for β-strands in the same color code. Dotted lines indicated loop regions. The eIF1A L65M mutation, used for the SAD data set, and the catalytic mutation of Ran Q69L are marked with a black rectangle. Interacting residues for Imp13 (green), Ran (yellow) and GTP (black), which were identified by the AquaProt server (Reichmann et al., 2007), are marked with colored circles above the sequence. For identifications of potential interacting residues of eIF1A with Imp13 and Ran, a MODELLER based model including all sidechains was analyzed with PISA (Krissinel and Henrick, 2007) and marked in the same color code with empty circles. Residues that were shown in co-precipitations to participate in the interaction, are marked with color-filled circles.

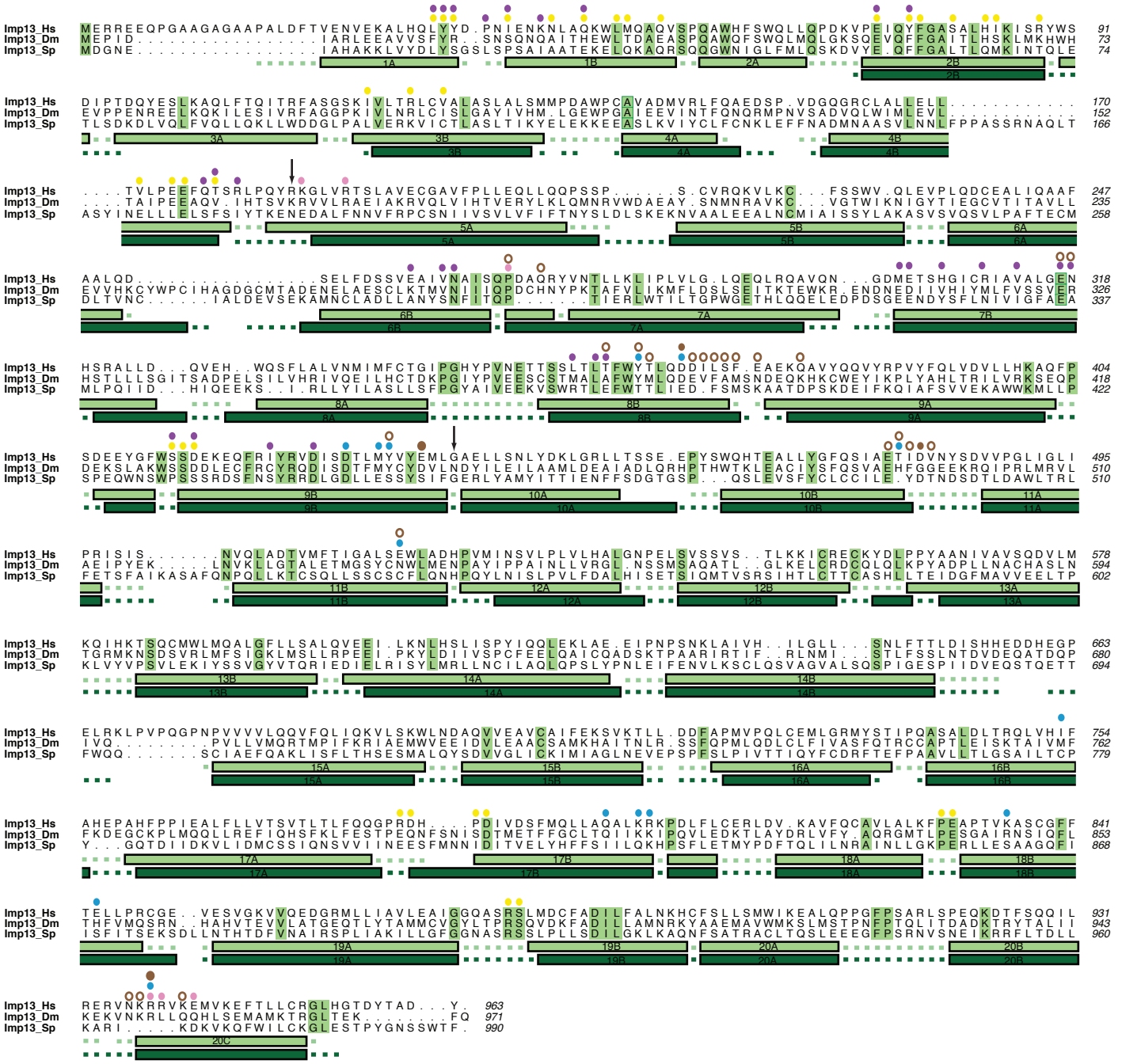

Supplementary Figure 1B. Structure-based sequence aligment of Imp13.
The alignment shows Imp13 orthologues from *H. sapiens* (Hs), *D. melanogaster* (Dm) and *S. pombe* (Sp). The conserved residues are highlighted in green. The HEAT-repeats of Hs and Dm Imp13 are shown below the sequence as light and dark green rectangles, respectively. Dotted lines represent loop regions. The two hinge regions of Imp13 are marked with a black arrow. Interacting residues for Ran (yellow), Ubc9 (purple), Mago (blue) and Y14 (magenta), which were identified by the AquaProt server (Reichmann et al., 2007), are marked with colored circles above the sequence. For identifications of potential interacting residues of eIF1A with Imp13, a MODELLER based model including all sidechains was analyzed with PISA (Krissinel and Henrick, 2007) and marked with empty brown circles. Residues, which were shown in co-precipitation to participate in the interaction, are marked with color-filled brown circles.

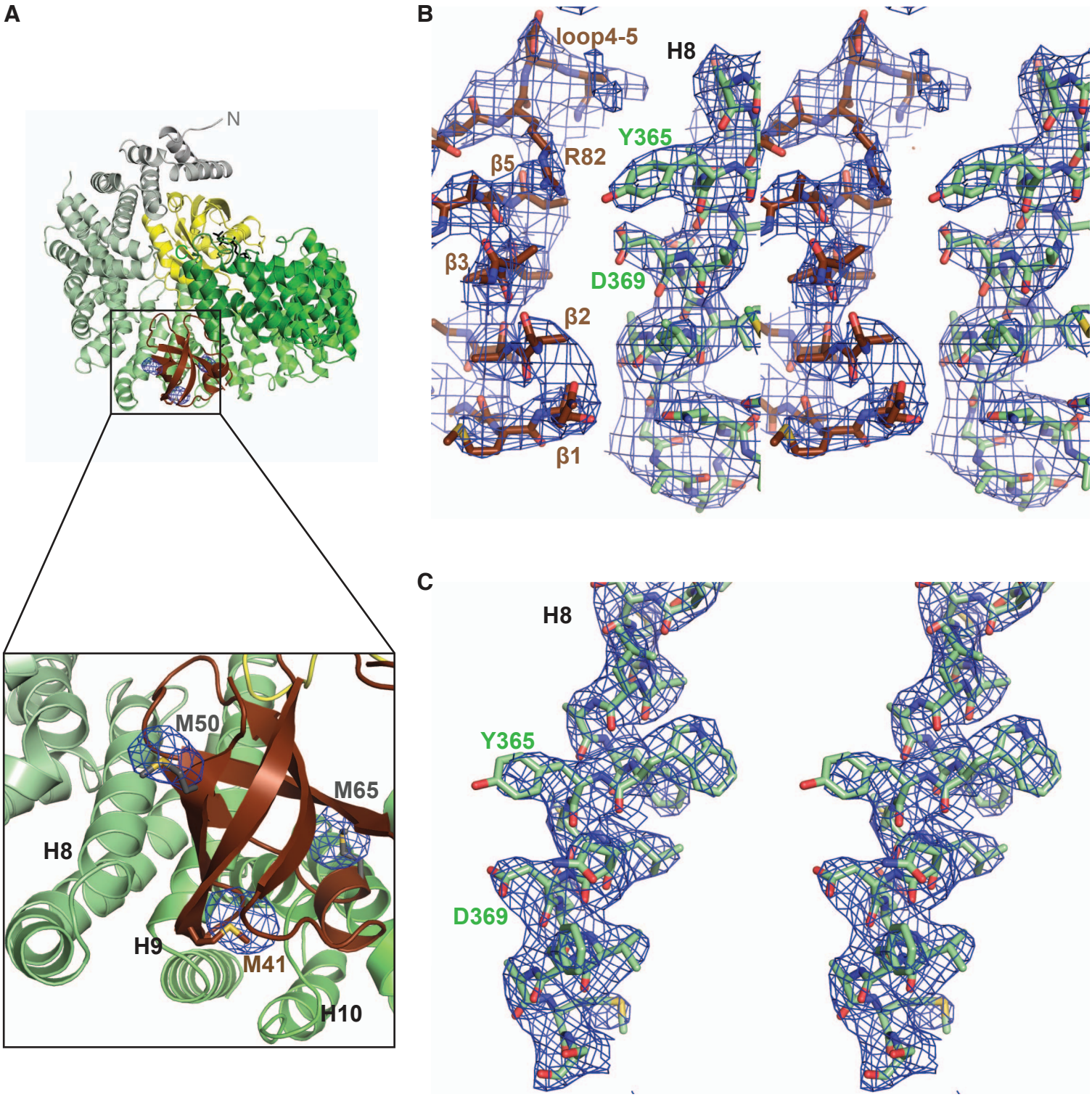

Supplementary Figure 2. Quality of the electrondensity. (**A**) Cartoon view and zoom-in (tilted) of the Imp13-RanGTP-eIF1A complex in the same color code and view as in Fig. 1A with an overlay of the anomalous Fourier map of the SeMet substitued eIF1A L65M SAD data set contoured at 4σ. The three methionine peaks of eIF1A L65M are shown as a blue mesh. The two methionine sidechains shown in coal were modeled in Coot (Emsley and Cowtan, 2004). (**B**) Stereo view of the eletron density of the 2Fo-Fc maps of the Imp13-RanGTP-eIF1A complex and of the Imp13 apo structure (**C**) after refinement and in a similar view. The interaction between Imp13 (green) and eIF1A (brown) is shown in a similar view as in Fig. 2A after a 180 rotation around the y-axis. The electron density is visualized as a blue mesh contoured at 1σ.

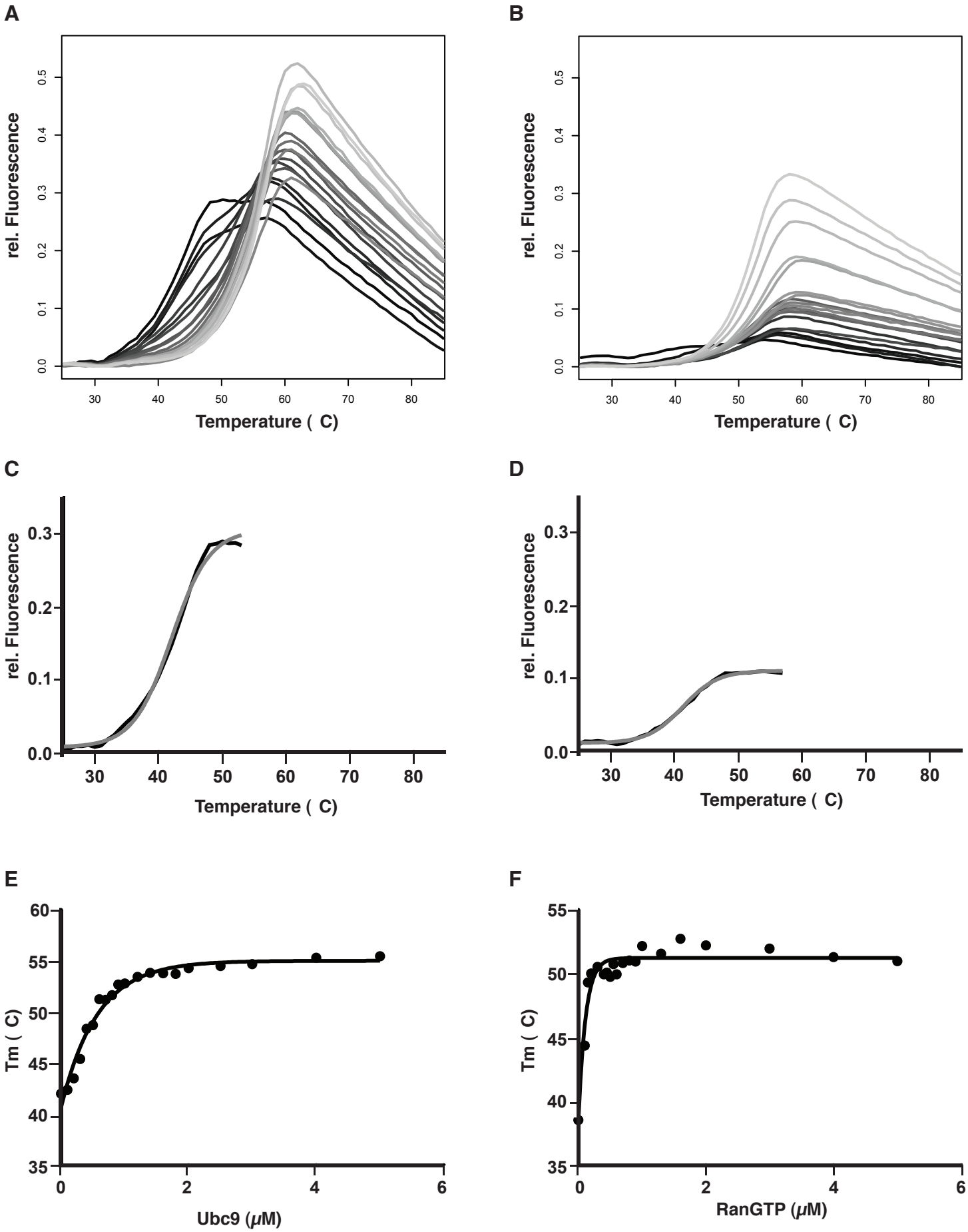

Supplementary Figure 3. Representative DSF curves. (**A**) and (**B**) show melting curves of Imp13 in dependence of increasing concentration of either Ubc9 (**A**) or RanGTP (**B**). The melting curves are plotted from black to gray according to increasing concentration of the ligand. (**C**) and (**D**) represent the melting curve of the first step of Ubc9 or RanGTP titration, respectively. The curves were fitted with the Boltzmann equation for the calculation of the Tm. (**E**) and (**F**) represent a plot of Tm against the concentration of Ubc9 (**E**) and RanGTP (**F**) with an exponential equation fitted. For the calculation of the K_D values, at least three independend measurement were carried out. Note that the RanGTP curve is too steep for a precise calculation of the K_D.

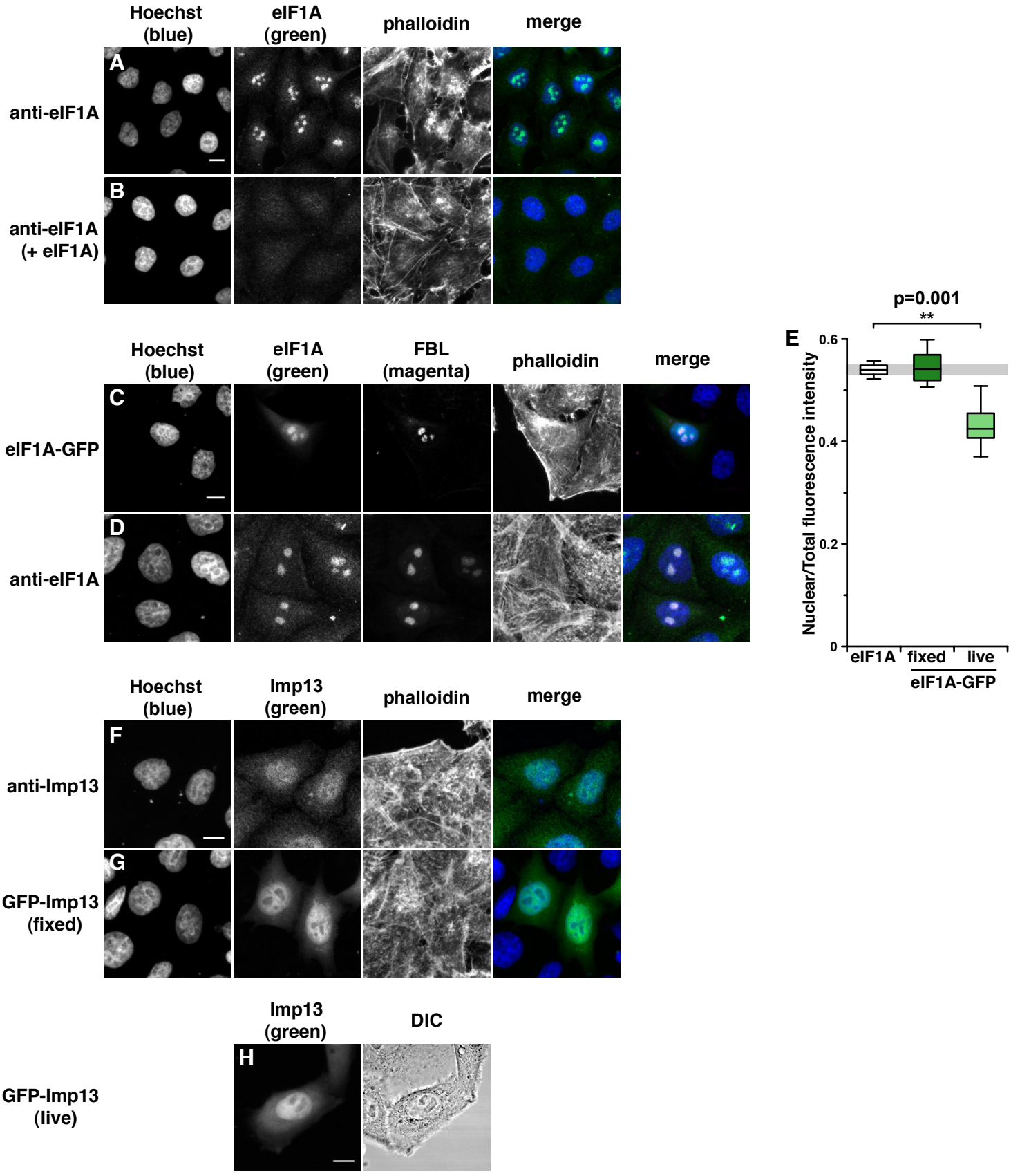

Supplementary figure 4. Localization of eIF1A and Imp13.
(**A-F**) Fluorescence microscopy images of fixed HeLa cells; the merged images show the nuclei (blue), the depicted endogenous or overexpressed protein (green) and, where indicated, the nucleolar protein FBL fused to mCherry (magenta). (**A, D**) Localization of endogenous eIF1A; in **B** the anti-eIF1A antibody was incubated with recombinant eIF1A prior to immunostaining. (**C**) Localization of GFP-tagged eIF1A (eIF1A-GFP). (**E**) Relative quantification of the fluorescence intensity in the nuclear compartment for endogenous eIF1A and eIF1A-GFP, both in fixed samples and live imaging (see also Fig. 5). (**F**) Localization of endogenous Imp13. (**G-H**) Localization of GFP-tagged Imp13 (GFP-Imp13) in fixed (**G**) and in live cells (**H**); DIC: differential interference contrast. At least three independent experiments were performed. Statistical significance was assessed with one tailed t-tests on the means of each experimental replicate, between the indicated conditions; the exact probabilities for alpha=0.05 are shown. (**) $p<0.01$, (*) $p<0.05$.Scale bar: 10µm.

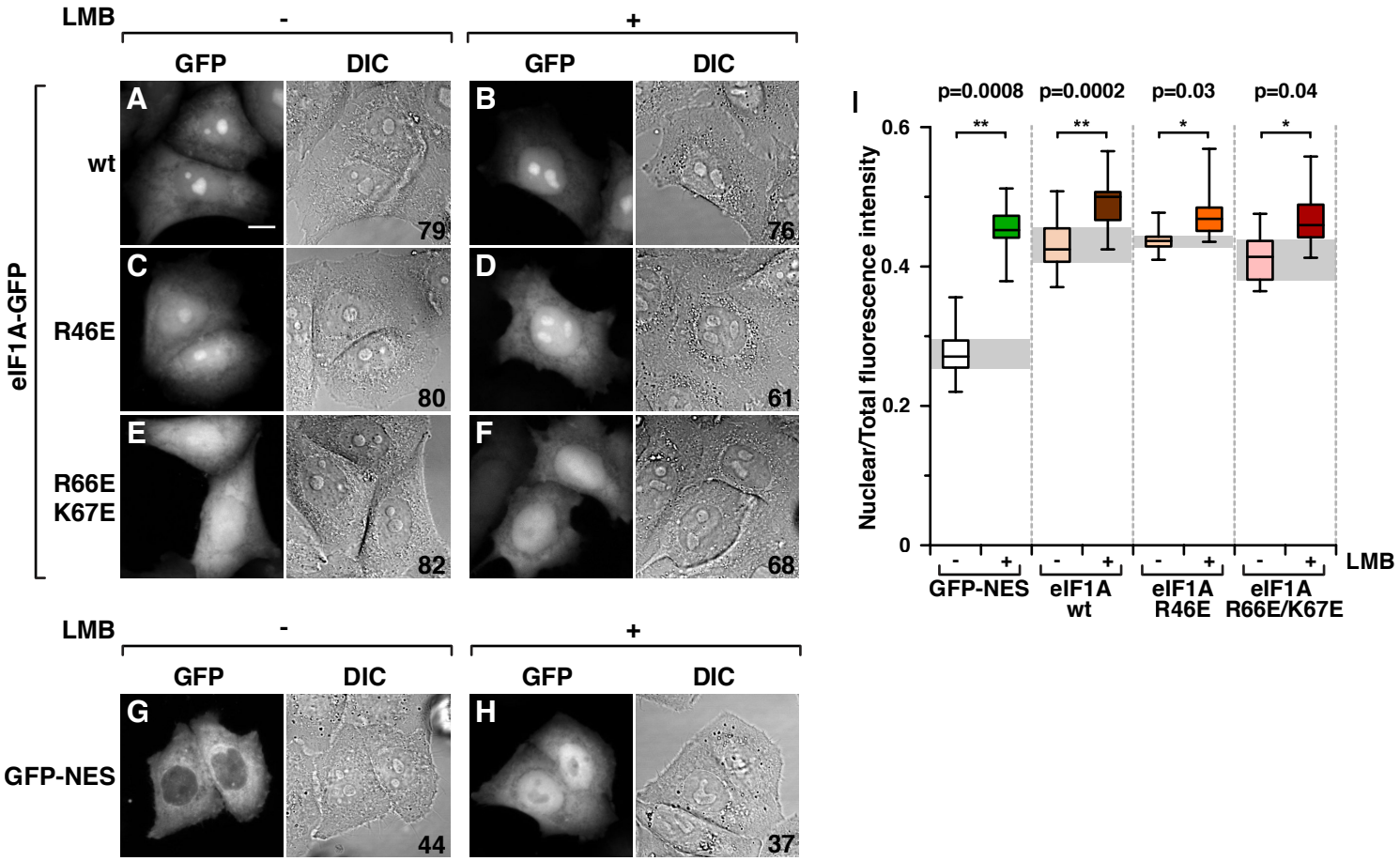

Supplementary Figure 5. CRM1 contributes to eIF1A localization.
(**A-H**) Fluorescence microscopy images and the corresponding DIC images of living HeLa cells expressing GFP-tagged eIF1A (eIF1A-GFP) wild type (wt, **A-B**) or mutants (**C-F**), or GFP fused to the nuclear export signal (GFP-NES) of the protein kinase A inhibitor (**G-H**). Localization of each construct in the absence (**A, C, E, G**) or presence (**B, D, F, H**) of Leptomycin B (LMB) is shown. (**I**) Relative quantification of the fluorescence intensity in the nuclear compartment for each construct, in the absence (-) or presence (+) of LMB. At least three independent experiments were performed; the number of analysed cells is indicated for each condition. Statistical significance was assessed with one tailed t-tests between the indicated conditions; the exact probabilities are shown. (**) $p<0.01$, (*) $p<0.05$. Scale bar: 10 µm.

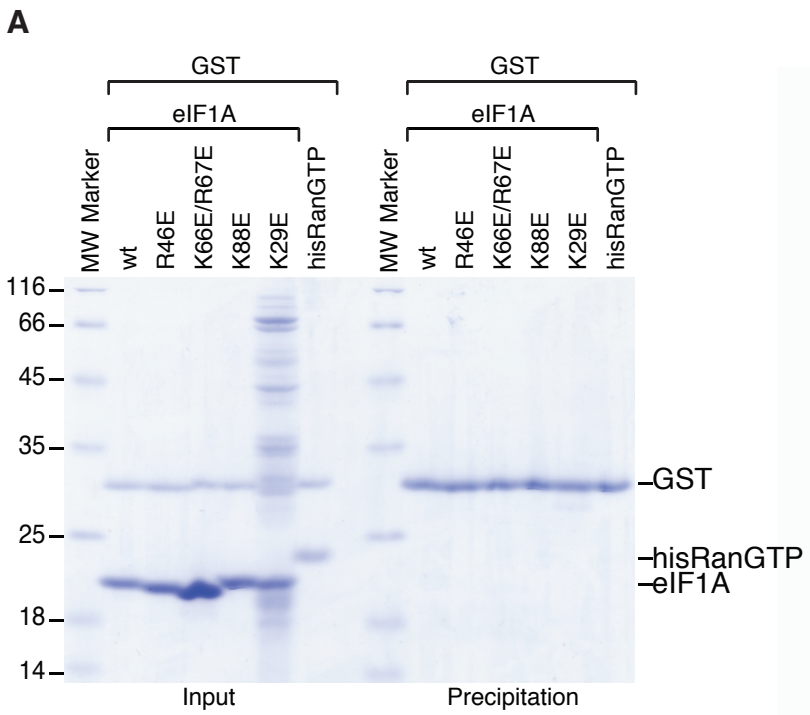

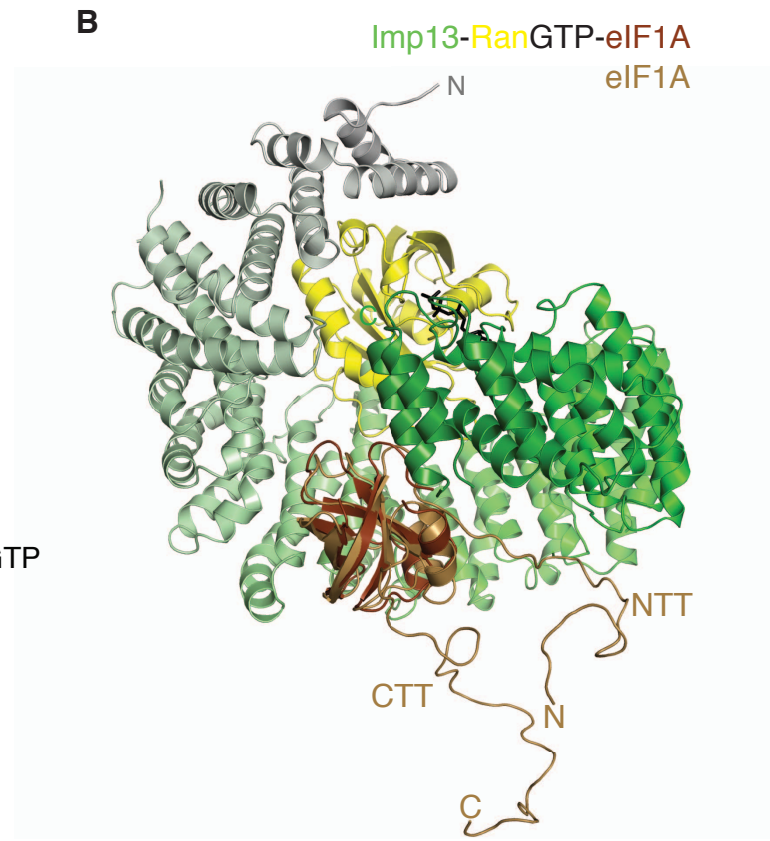

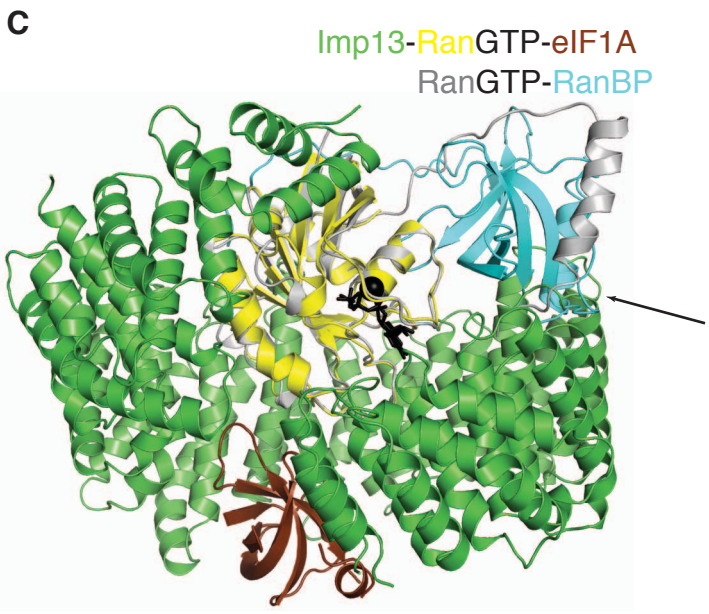

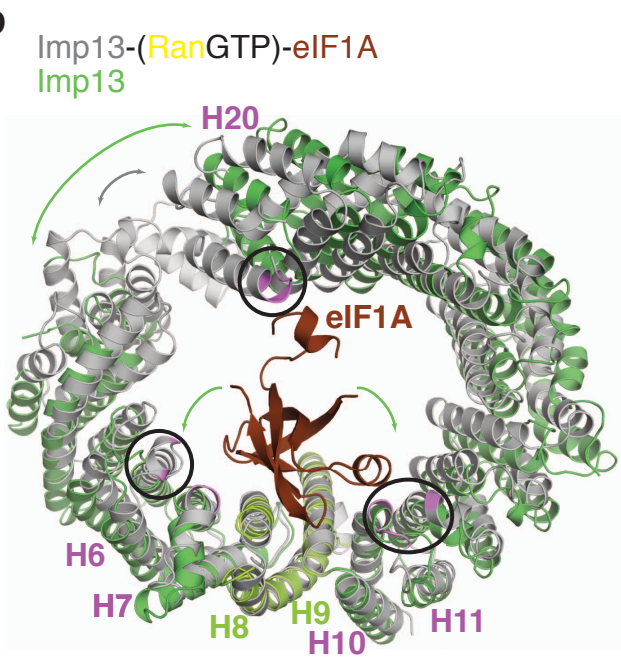

Supplementary Figure 6. (**A**) Protein co-precipitation by GST incubated together with RanGTP and eIF1A either with wild type (wt) or mutant. For the input control 1/6 of the samples were kept (upper panel) and the rest was co-precipitated with glutathione sepharose beads and analyzed on Coomassie stained 15 % SDS-PAGE. The far left lane was loaded with a molecular weight marker. Refers to Figure 2c (**B**) Cartoon view of a superposition of the NMR solution structure of human eIF1A (sand) (pdb id.: 1d7q) (Battiste et al., 2000) to eIF1A in the trimeric export complex Imp13-RanGTP-eIF1A. The Imp13-RanGTP-eIF1A structure is shown in the same color code and view as Figure 1b. (**C**) Superposition of Imp13-RanGTP-eIF1A with RanGTP-RanBP structure (pdb id: 1rrp)(Vetter et al., 1999), in grey and in cyan, respectively (**D**) eIF1A binding site on Imp13 apo and on Imp13 in the trimeric complex. Imp13 unbound is in green and in the export complex in grey, eIF1A is in brown and RanGTP is not shown for clarity. In pale green, the portion of eIF1A binding-site optimally superposed. Other interaction sites between Imp13 and eIF1A in the export complex are labeled in pink. Circled in red eIF1A interactions lost in the Imp13 apo conformation. Arrows highlight the compacting movement between the two Imp13 states.

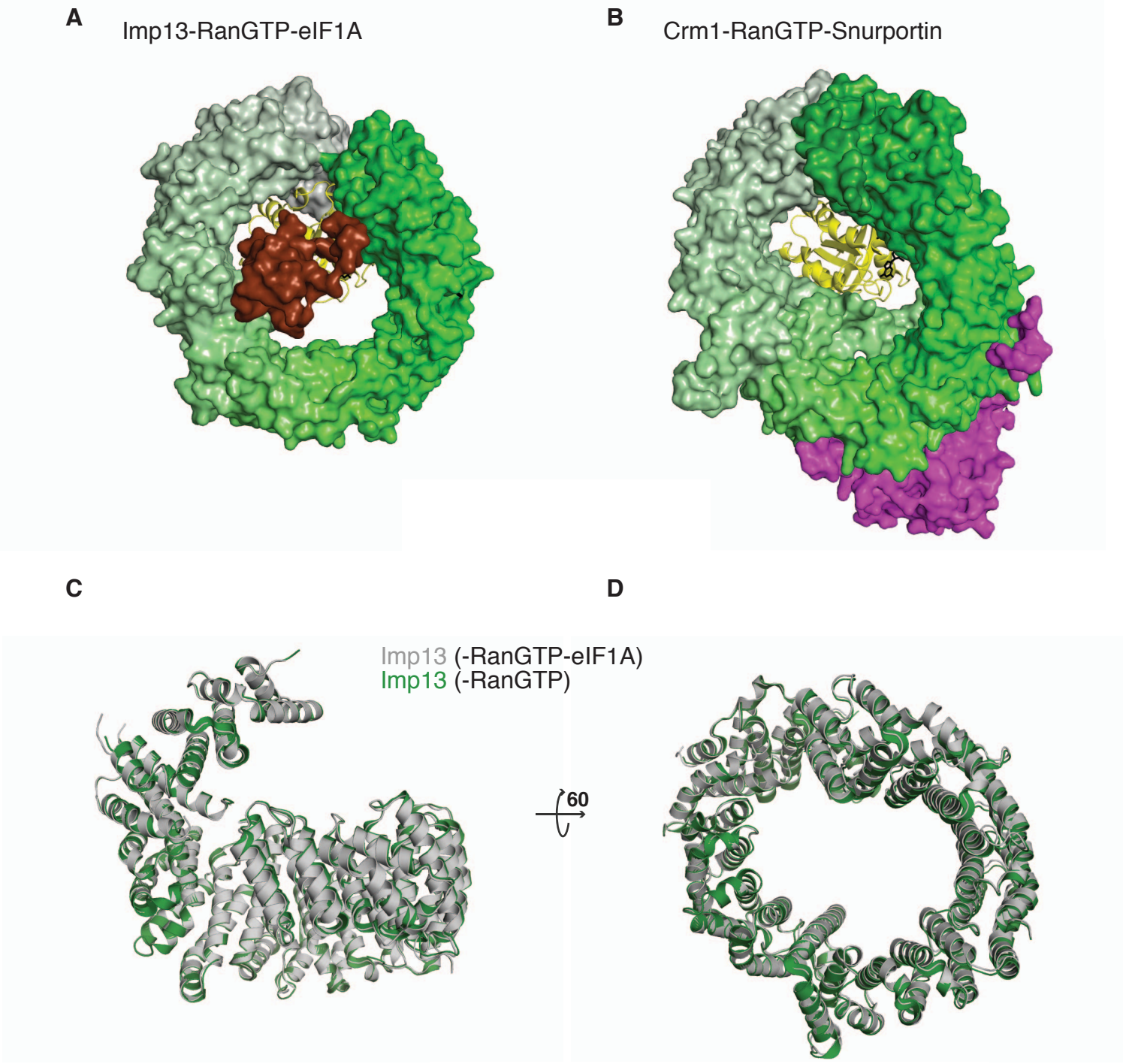

Supplementary Figure 7. Comparison of different karyopherin complexes.
A) and **B**) Surface view of different export-complexes in a similar view as in Fig1B turned 180 around the z axis. The exportins are shown in a gray to green color gradient. Ran is visible as yellow cartoon with the bound GTP in black. The export cargo eIF1A (**A**) is rendered as a surface in brown, while Snurportin bound to Crm1 (**B**) (Monecke et al, 2009; pdb id.: 3gjx) is in magenta. **C**) and **D**) Cartoon representation of Imp13 in complex 3 superposed to Imp13 in the previously described binary complex (Bono et al., 2010; pdb id.: 2x19) in a similar view as in Fig. 1B, C. Other components of the complexes are removed for clarity.